Simulation results for light propagation in the central detector: 3-dimensional case

T. A. Alvarenga, A. F. Barbosa, L. M. A. Filho, R. A. Nobrega
Universidade Federal de Juiz de Fora - UFJF
Centro Brasileiro de Pesquisas F/isicas - CBPF
e-mail:rafael.nobrega@ufjf.edu.br

Abstract

An antineutrino detector to be installed in the area surrounding the Angra II nuclear reactor in Angra dos Reis is currently under development. The related experiment is intended to measure the antineutrino flux coming from the reactor, making use of a detection system placed near the reactor dome, and correlate it to the nuclear fuel fission and burn-up. The proposed detector is a box-shaped volume filled with water and doped with Gadolinium. The photons generated by the passage of particles in the target volume are collected by photomultiplier tubes (PMT). Aiming to evaluate the importance of reflecting inner surfaces and to provide directives concerning the best positioning of the PMTs inside the detector, a Monte Carlo simulation of light propagation in the active volume has been done. Photons are supposed to be point-like entities traveling in straight lines. We investigate the overall photon counting efficiency by analyzing the number of reflections and the length traveled by the photons before being collected or absorbed, as well as the distribution of these photons in different configurations of the PMTs. Different light reflecting structures around the PMTs are also simulated, in order to find those that reduce the probability for a photon to be bounced back to the direction from which it was emitted. We show that a configuration in which the photon emission direction is preserved may be used as veto for cosmic events.

1 Introduction

The basic geometry proposed for the target detector of the Neutrinos-Angra project [1] has been initially defined as a cubic shape with 40 Hamamatsu R5912 [2] PMTs distributed over its walls as shown in Figure 1. The detector dimensions define an internal target volume of approximately 1 ton. The volume will be filled with a mixture of highly pure water and a small percentage of gadolinium.

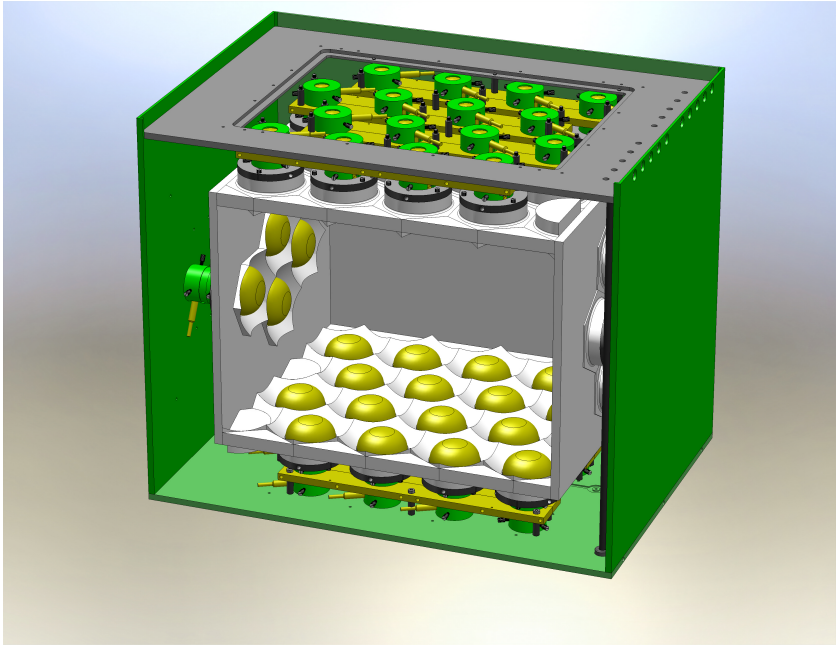

Figure 1: View of the latest technical drawing for the central detector.

In this document we present results taken from a simple Monte Carlo simulation to study how the photon detection performance is affected by varying some of the detector geometric characteristics. The main geometric variations to be addressed are: shifting the positioning of the top PMTs, exchanging the rows order; adding reflective structures around the PMTs in order to increase the probability of capturing a photon when it hits the wall in a region close to a PMT; taking out the lateral PMTs from the target volume. The main parameters used to evaluate the different geometries are based on the occupancy of captured photons over the PMTs; the efficiency of detecting a photon once it is emitted inside the detector, per crossed length or per number of reflections; and the bottom/top ratio of detected photons, which can help as a veto for cosmic ray events. The photons can be generated isotropically inside the detector, as expected for the anti-neutrinos reaction ($\overline{\nu} + p \rightarrow e^{+} + n$) and externally, following the cosmic rays angular distribution. An exponential probability density function based on the average range parameter, which represents the average distance travelled by the photon, is also considered in the simulation. This parameter is also programmable, since it depends on currently unknown detector characteristics as the water purity and the concentration of gadolinium.

The two-dimensional case has been studied previously [3]. In this note we expect to get new and more realistic results once the detector geometry and the photon propagation will be described in 3 dimensions. In the next section, the main characteristics of the software is described. Following is a section where the achieved results are presented.

2 Software

A toy Monte Carlo simulation of light propagation inside the target detector has been developed. The software is based on C++ and makes use of the ROOT framework [4], which is an object-oriented programming environment containing a set of libraries which allows, among other facilities, the creation of specific geometries, the generation of random data following specific probability density functions (pdf), and the propagation of particles within any created geometry world.

Figure 2 shows the main panel for the ROOT based developed software. The main programmable parameters are available on the panel. They will be better explained throughout the text. Visualization of events is also possible as shown at the right side of this figure.

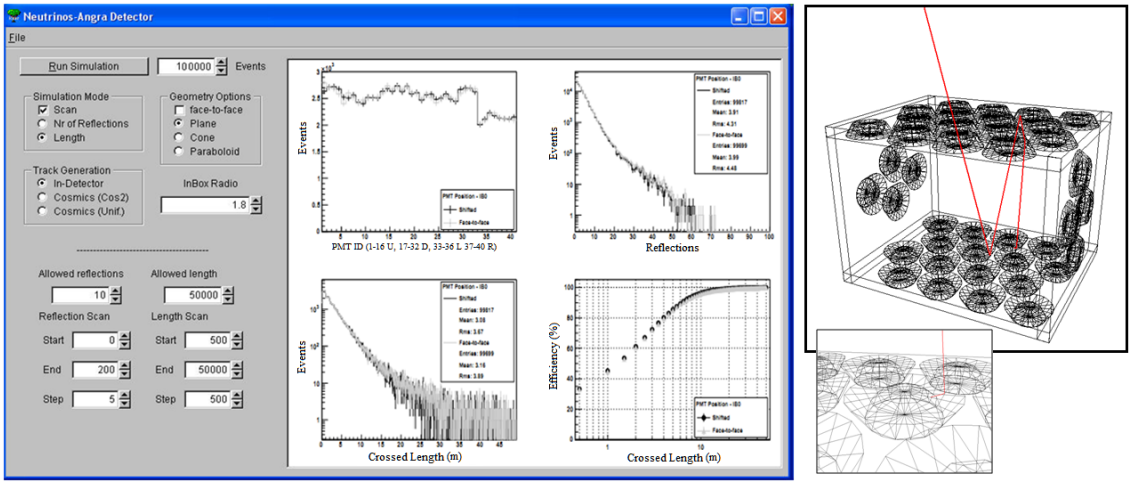

Figure 2: Main panel of the ROOT based developed program after a simulation run (left) and detailed visualization of one event (right).

2.1 Geometry

Figure 3 shows the skeleton of the target detector as implemented in the software. In this figure, the detector is equipped with all the 40 PMTs and its walls are flat. Figure 4 shows the walls with the addition of an internal structure surrounding the PMTs. Two structure types have been considered: with conic and in paraboloid shapes. The external radius of those shapes has a fixed value, near to the larger PMT radius, while the value of the internal radius is adjustable. The unit used for the internal radius is based on the external radius; e.g. 1 means that the internal radio is equal to the external one. As an example, Figure 4 shows the detector with two different internal radio values for those structures.

Another possible geometry variation is the positioning of the top and bottom PMTs. Two configurations have been considered: face-to-face and shifted. The former considers that each bottom PMT is facing a top PMT as shown in the left illustration of Figure 5. At right it is shown the shifted configuration.

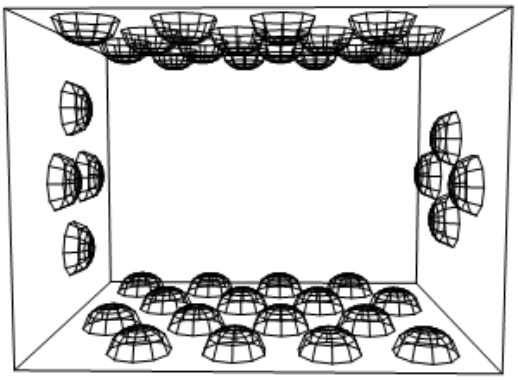

Figure 3: Representation of the target volume detector in the software environment.

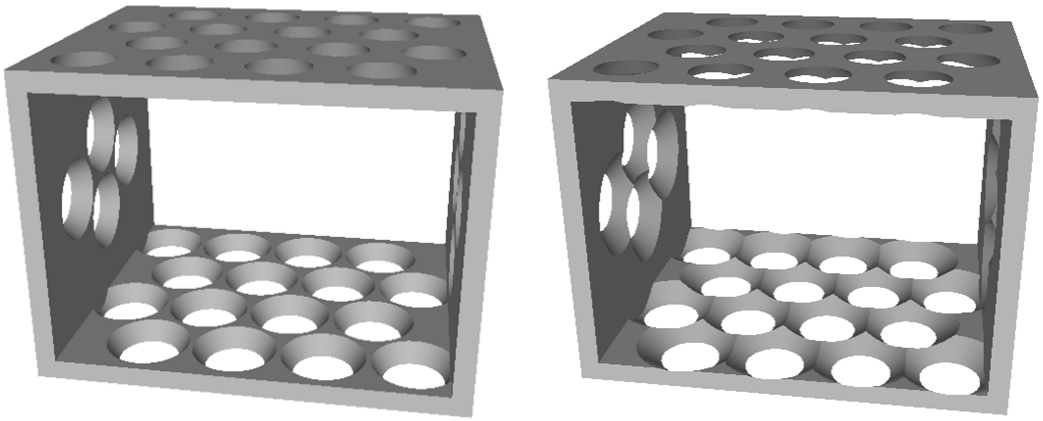

Figure 4: Radii factors 1.2 (left) and 1.8 (right) used to the internal structures surrounding the PMTs.

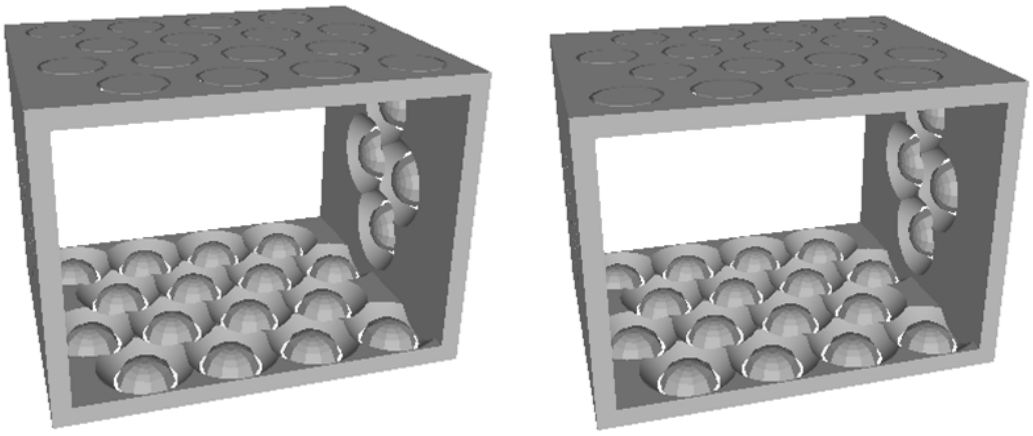

Figure 5: At left, each PMT located at the bottom of the target detector is facing a PMT located at the top. At right, those PMTs are shifted.

2.2 Photon Generation

Three options were implemented for photon generation; two external to the detector, representing *Uniform* and Cos^2 cosmic rays and one internal to the detector, isotropically distributed in location and direction, called generation In-Detector. The Cos^2 option respects the angular distribution of cosmic muons at sea level described by a $cos^2\theta$ function where θ is the zenith angle, varying from -$\pi/2$ to $\pi/2$. As an example, Figure 6 shows photons being generated inside the detector and outside the detector, respecting the cosmic rays direction distribution.

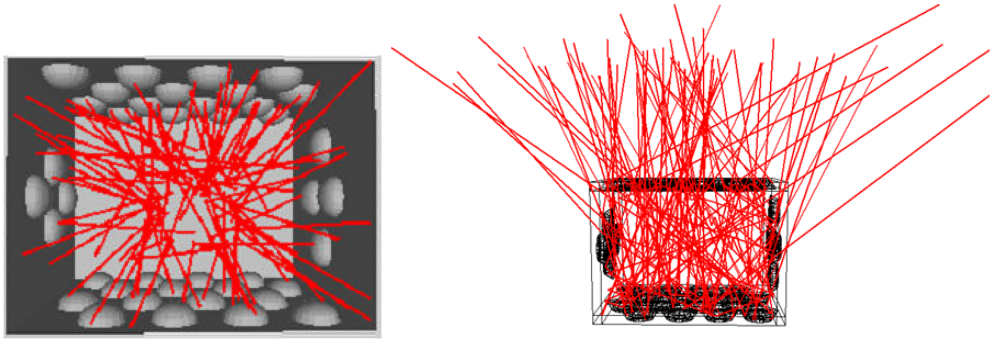

Figure 6: Photons being generated isotropically inside the target detector (left), and following the cosmic rays directions distribution (right).

The distance traveled by the photon is also programmable; three options have been implemented considering that a photon emitted inside the detector is absorbed when: a certain number of reflections is reached; when a given length is traveled; or according to a length distribution taken from a pdf based on a programmable average range value, which depends on the characteristics of the water which will be used in the target detector volume. It should be noted that the number of allowed reflections can be set to zero, which corresponds to the example shown at the left of Figure 6. For completion of this study, the option where only the side walls are reflective was also implemented.

3 Detector Walls Effect Evaluation

3.1 Detector without Internal Structure (Plane Walls)

Figure 7 shows the results obtained for a detector with plane walls and shifted top-bottom PMTs (face-to-face top-bottom PMTs) and for photons created isotropically inside the detector. The top-left plot shows how the hits are distributed over the PMTs, according to the PMT mapping. The top-right plot shows the distribution of the number of reflections needed for the photon to hit a PMT; In average the photon needs 3.91 (3.99) reflections before hitting a PMT. The bottom-left plot shows the length crossed by the photon before hitting a PMT; in average, the photon travels 3.08 m (3.16 m) before hitting a PMT. The bottom-right plot shows the efficiency per crossed length: up to 1 m, 45.1% (44.6%) of the events hit the PMT; up to 2 m, the efficiency increases to 61.1% (60.5%); up to 4 m, it goes to 80.1% (79.6%) and up to 7 m, the efficiency reaches 92.0% (91.5%). An efficiency of 99% is reached for a maximum distance of 19 m (22 m). Using a face-to-face or shifted positioning has no practical difference in any of the graphics presented in this figure.

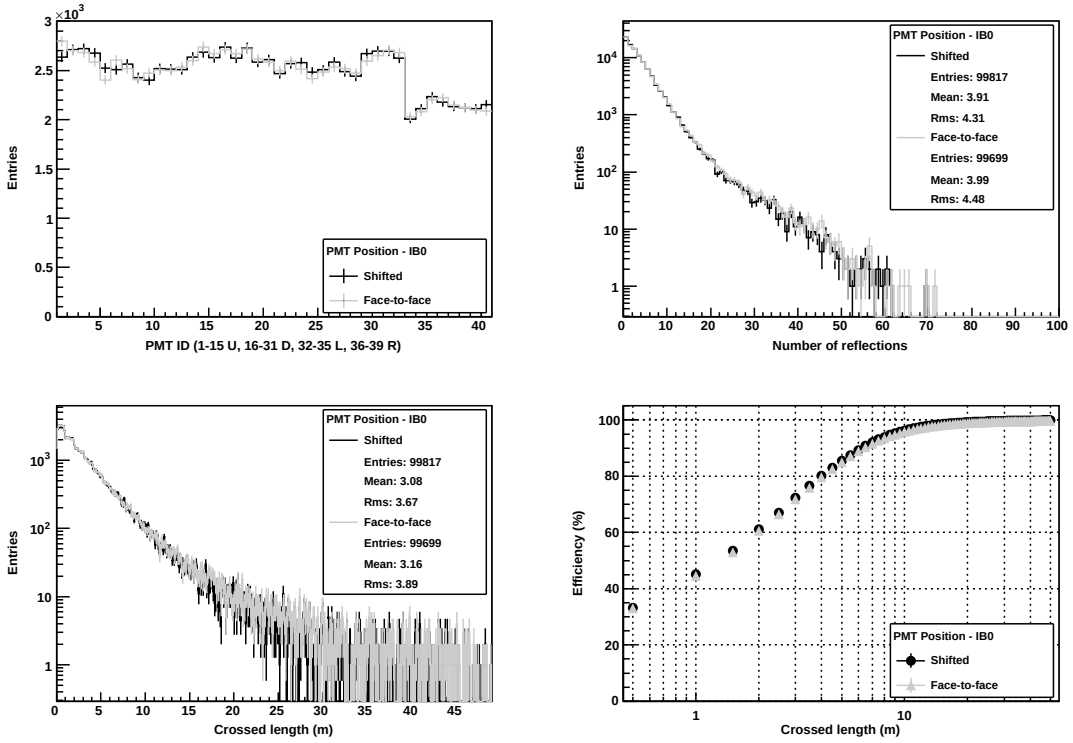

Figure 7: Results from a run with 100000 events uniformly distributed inside the detector without internal box structure.

The number of reflections needed for a photon to hit a PMT has also been evaluated. Approximately, 23% of the events hit the PMT without any reflection; with up to 2 reflections, the efficiency increases to 54% and up to 10 reflections it amounts to 94%. The computed average for the number of reflections are: 3.978 ± 0.015 for photons generated isotropically inside the detector; 3.806 ± 0.023 for uniform cosmic generation; and 3.709 ± 0.022 for $cos^2\theta$ cosmic generation.

3.2 Internal Structure around PMTs

In this case, in which a geometric structure surrounds each PMT, it must firstly be chosen the radius of the hole to be used at the internal surface. Considering initially the measurement of the number of reflections needed for a photon to hit a PMT, it can be seen in Figure 8, for the conic shape at left and paraboloid shape at right, that this number is lower for radii values between 1.6 and 2.0, depending on the particular way the photons are generated.

Figures 9 and 10 show that the best radius values to identify photons coming from cosmic rays, lays around 1.6. Around this value, the bottom/top PMT hit ratio for photons generated by cosmic particles is maximized.

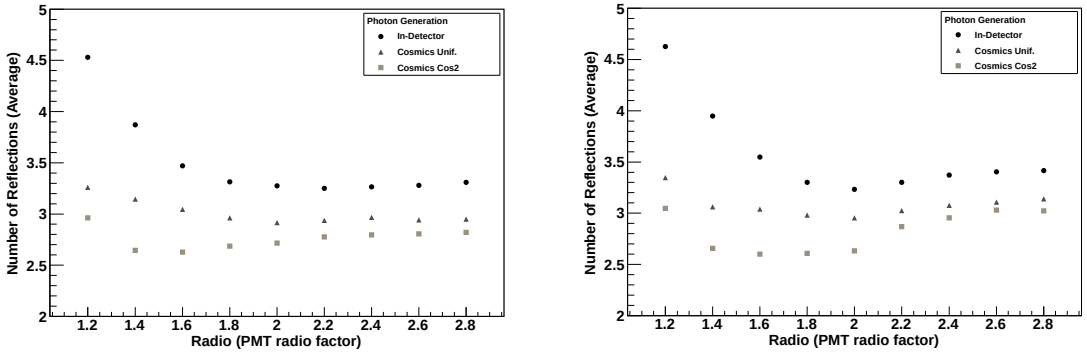

Figure 8: Average of number of reflections versus radius of the hole surrounding PMTs for photons generated inside and outside the detector, for cosmic rays, respecting uniform and $cos^2\theta$ distributions. The left plot shows the case of cone shaped holes, the right plot shows the case of paraboloid shaped holes.

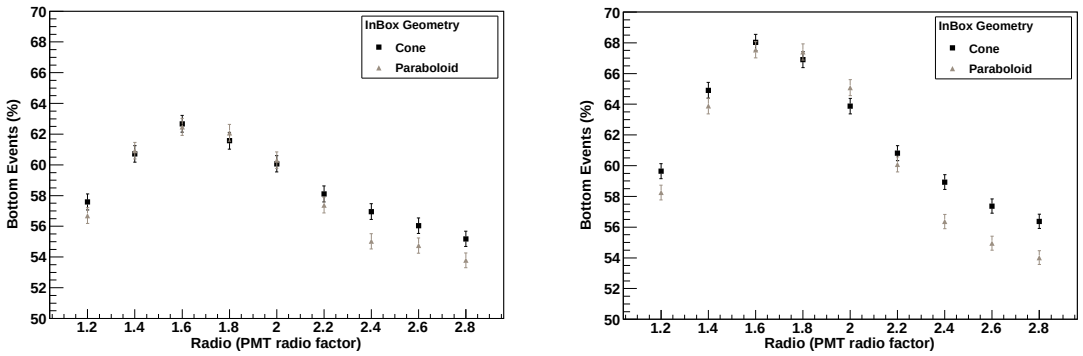

Figure 9: Percentage of bottom events for cosmic rays events for uniform distribution (left), and the same information is for the $cos^2\theta$ distribution (right).

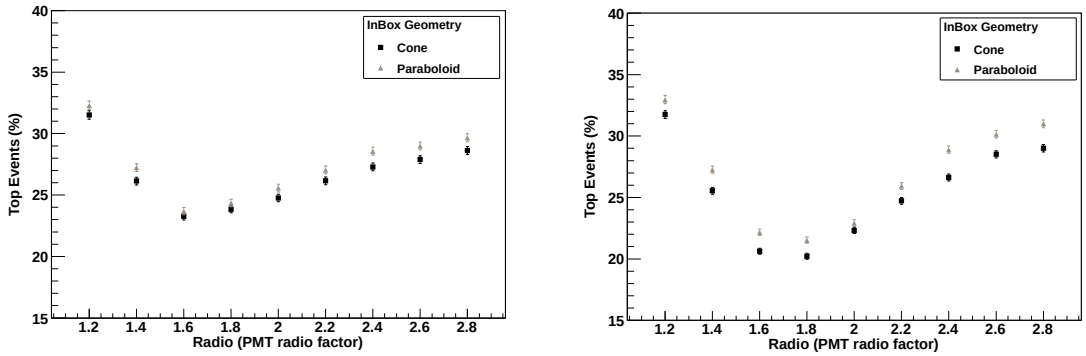

Figure 10: Percentage of top events for cosmic rays events for uniform distribution (left), and the same information for the $cos^2\theta$ distribution (right).

Figures 11 and 12 consider cosmic related events in their descending trajectory only, as if only the lateral walls were reflective. As it can be seen, the best results were reached for a radius factor between 1.4 and 1.6, as follows: 52% and 56% efficiency for photons generated as cosmic rays with uniform and $cos^2\theta$ distributions respectively; from the captured photons, 85% and 90% were captured by the bottom PMTs; the missing photons were captured either by the lateral PMTs or, in smaller proportion, by the top PMTs, which happens mainly when the arrived event enters the detector with a large horizontal component. Those values can be compared with the results obtained for the case where the detector walls are plane, summarized as follows: 39.7 % and 36.5 % of efficiency for photons generated as cosmic rays with uniform and $cos^2\theta$ distributions respectively; from the captured photons, 76% and 81% were captured by the bottom PMTs.

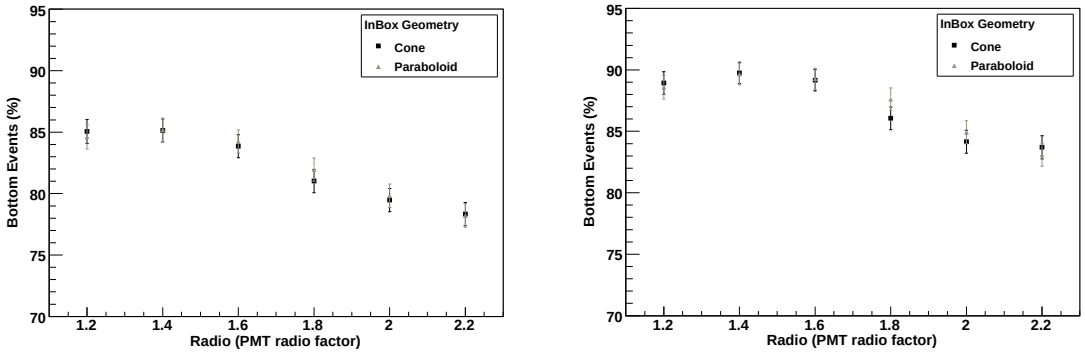

Figure 11: Percentage of bottom events for cosmic rays events (descending trajectory) for uniform distribution (left), and the same information for the $cos^2\theta$ distribution.

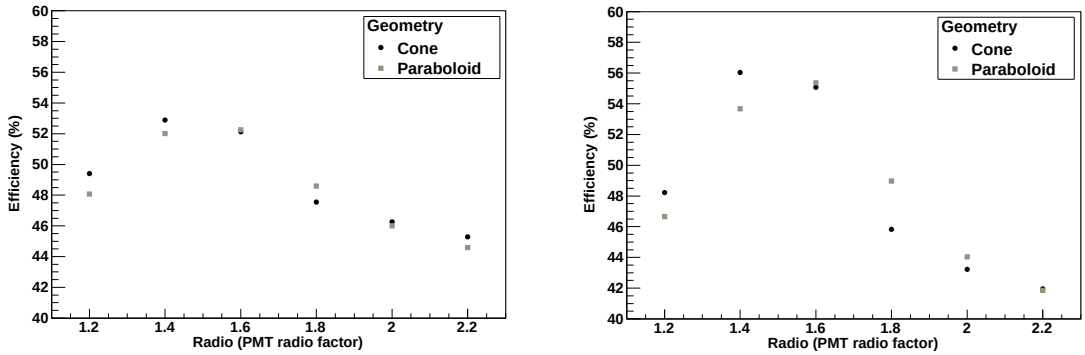

Figure 12: Efficiency versus internal holes radius for cosmic events (descending trajectory) for uniform distribution (left), and the same information for the $cos^2\theta$ distribution.

Figures 13, 14 and 15 show the efficiency gain, when comparing with the plane walls detector, according to the PMT radius factor and the number of reflections needed for to the photon to hit a PMT. According to these results, it can be concluded that the best PMT radio factor should be around 1.6. Therefore, this value will be used in the following measurements when not specified.

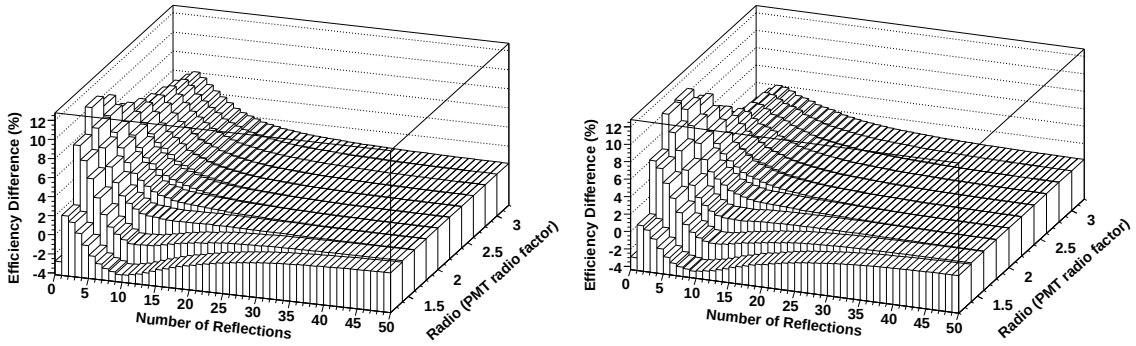

Figure 13: Efficiency improvement when using an internal structure in cone (left) and paraboloid (right) shapes in respect to plane walls for photons generated isotropically inside the detector.

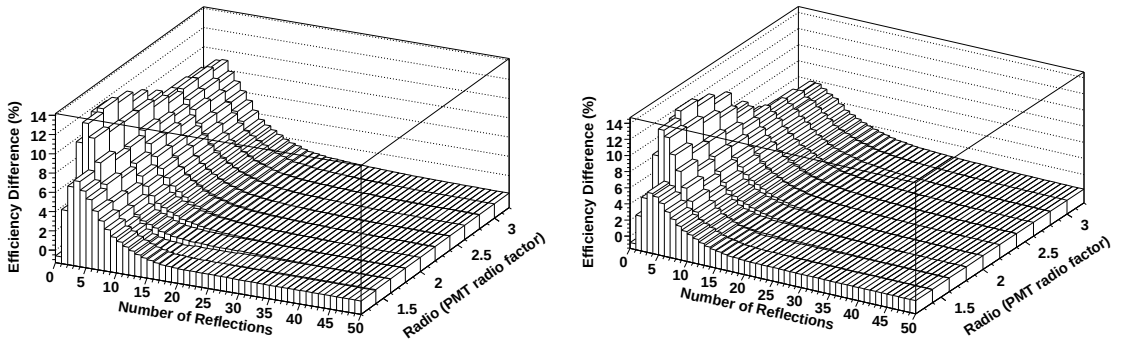

Figure 14: Efficiency improvement when using an internal structure in cone (left) and paraboloid (right) shapes in respect to plane walls for photons generated as cosmic rays with uniform distribution.

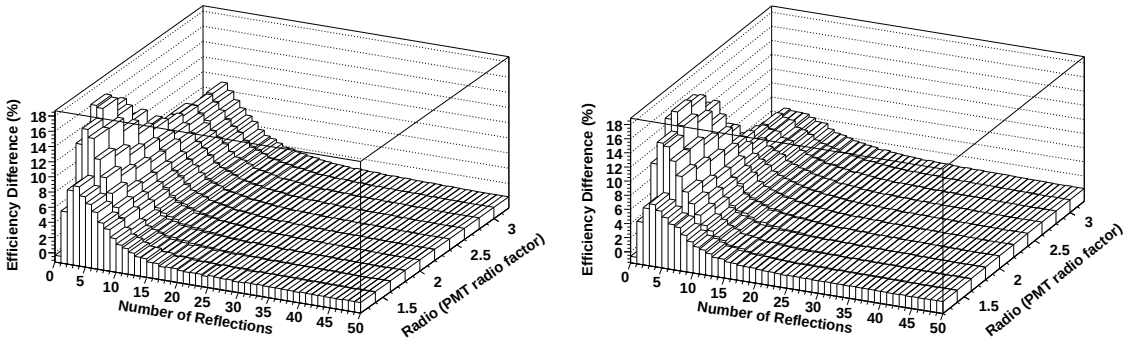

Figure 15: Efficiency improvement when using an internal structure in cone (left) and paraboloid (right) shapes in respect to plane walls for photons generated as cosmic rays with cos^2 distribution.

Once the PMT surrounding structure shape has been defined, we can present the final values comparing the different wall structures for different average ranges for the photon. Figures 16, 17 and 18 show these results.

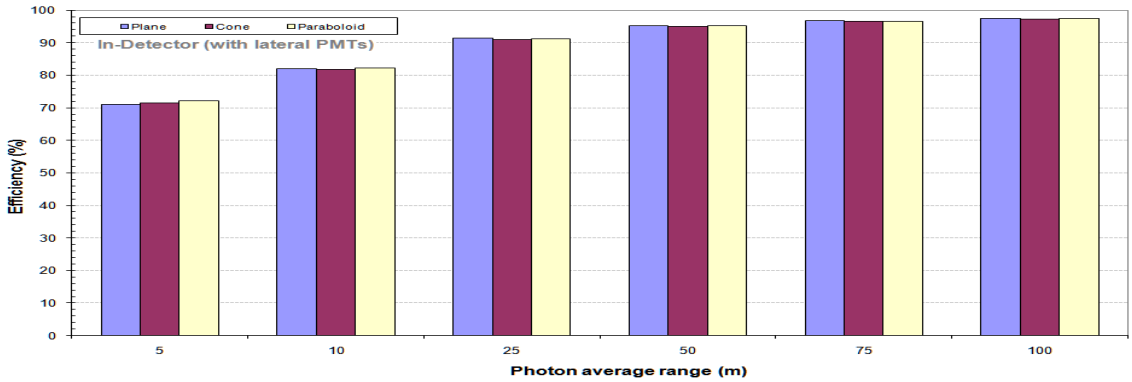

Figure 16: Efficiency for photons generated isotropically inside the detector.

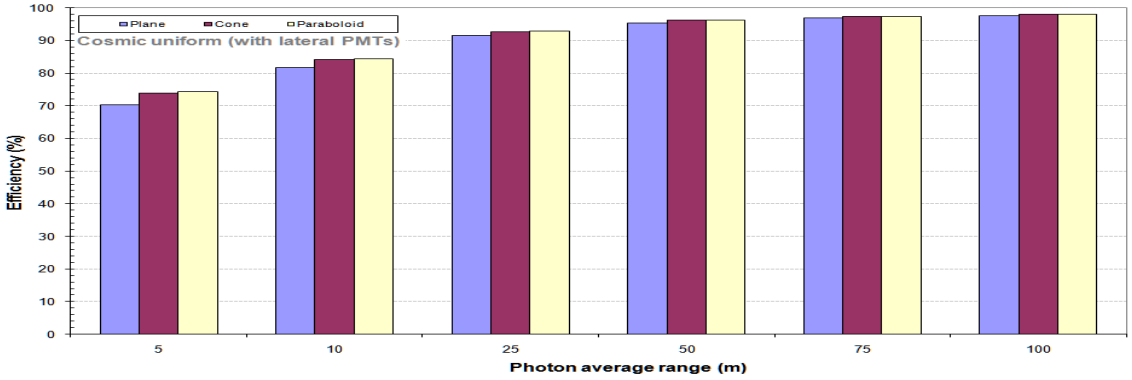

Figure 17: Efficiency for photons generated as cosmic rays with uniform distribution.

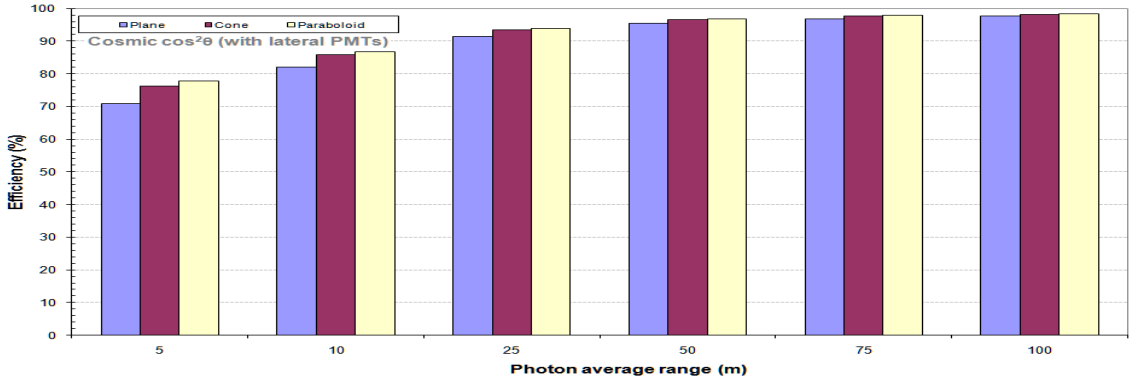

Figure 18: Efficiency for photons generated as cosmic rays with ccos^2 distribution.

As it can be seen, an internal structure (cone or paraboloid) can have significant effect on the detection efficiency for cosmic events for short average range; for values higher than 25 meters, its

importance is reduced. For events generated isotropically inside the detector, the effect is negligible. In the next section we show that the internal structure becomes slightly more important when the lateral PMTs are not used.

4 Lateral PMTs Evaluation

Figures 19, 20 and 21 show the percentage of the photons captured by the three PMT groups classified as bottom, top and side. Each set of 6 bins represents the following wall configurations: plane, cone and paraboloid, respectively, where each bin represents a different average range given for the photon. Figures 22 and 23 correspond to measurements performed without the lateral PMTs. As it can be verified, using or not the lateral PMTs does not change significantly the ratio of top to bottom events, while using an internal structure surrounding the PMTs, in cone or in paraboloid shape, increases this ratio. This information may help identifying photons generated by cosmic rays. In addition, the importance of the lateral PMTs is minimized when an internal structure is used. Nevertheless, as shown in the Figures 24, 25 and 26, for an average range higher than 25 meters, the use of lateral PMTs is not essential from the point of view of detection efficiency.

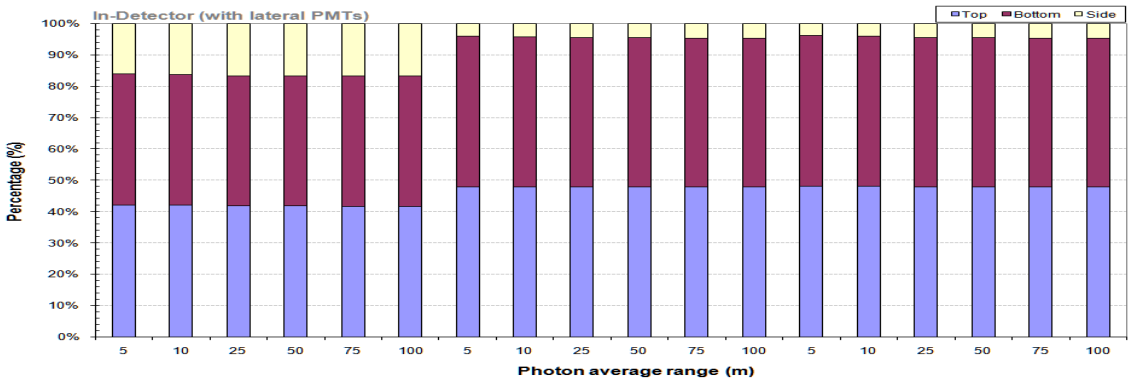

Figure 19: Efficiency for photons generated isotropically inside the detector.

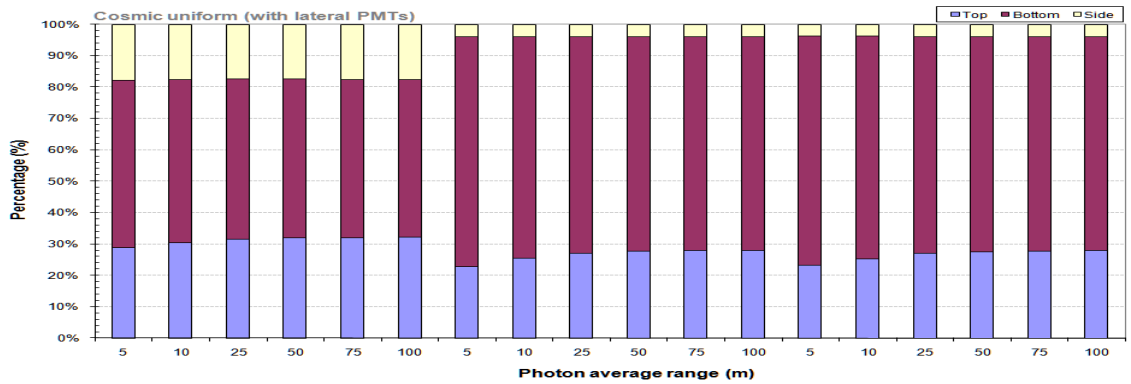

Figure 20: Efficiency for photons generated as cosmic rays with uniform distribution.

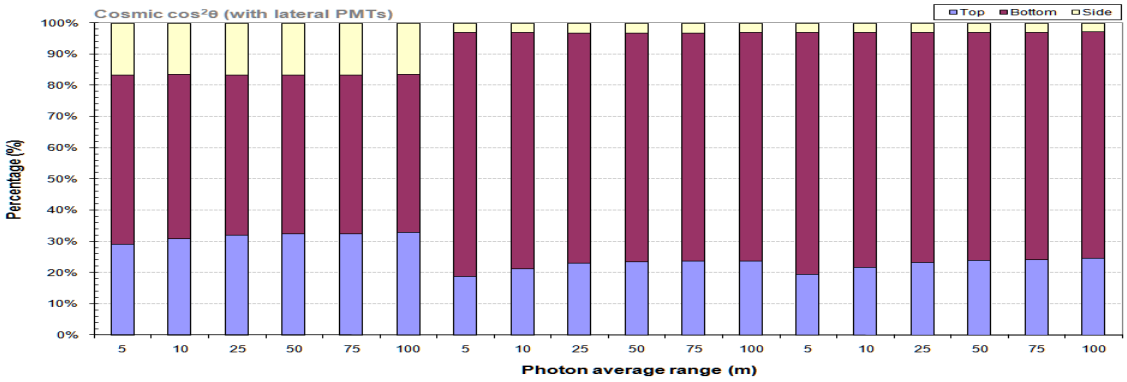

Figure 21: Efficiency for photons generated as cosmic rays with $cos^2\theta$ distribution.

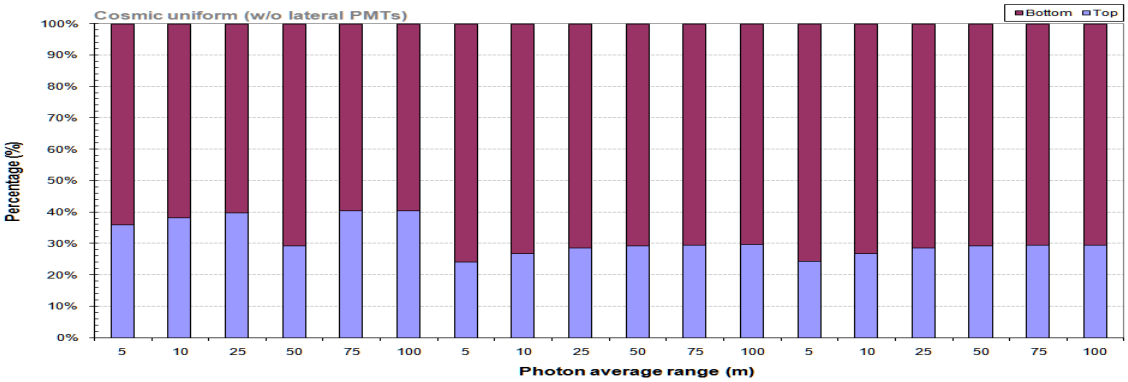

Figure 22: Efficiency for photons generated as cosmic rays with uniform distribution.

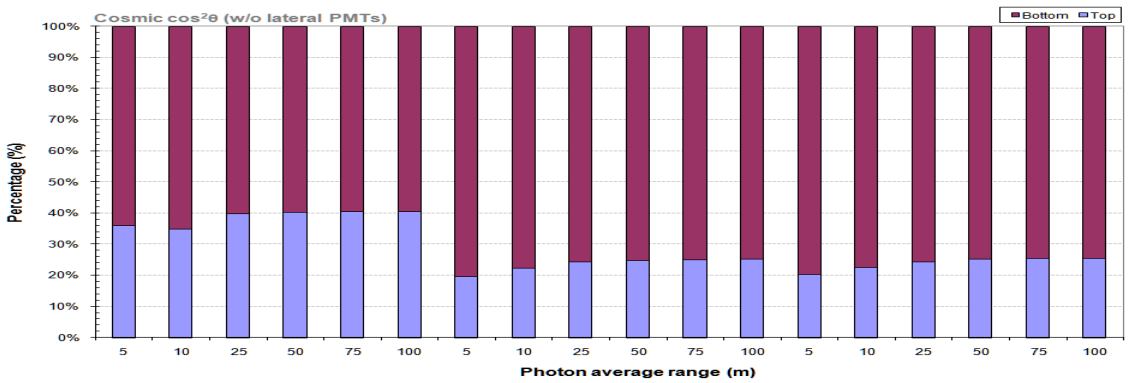

Figure 23: Efficiency for photons generated as cosmic rays with $cos^2\theta$ distribution.

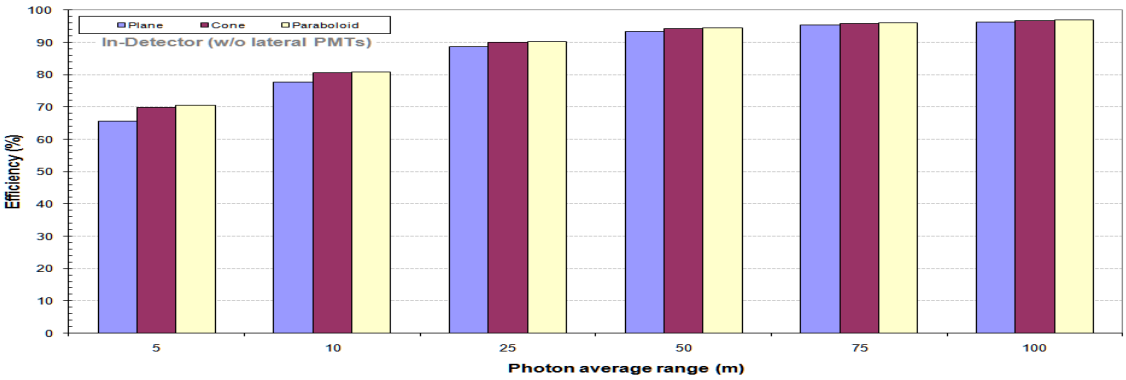

Figure 24: Efficiency for photons generated isotropically inside the detector.

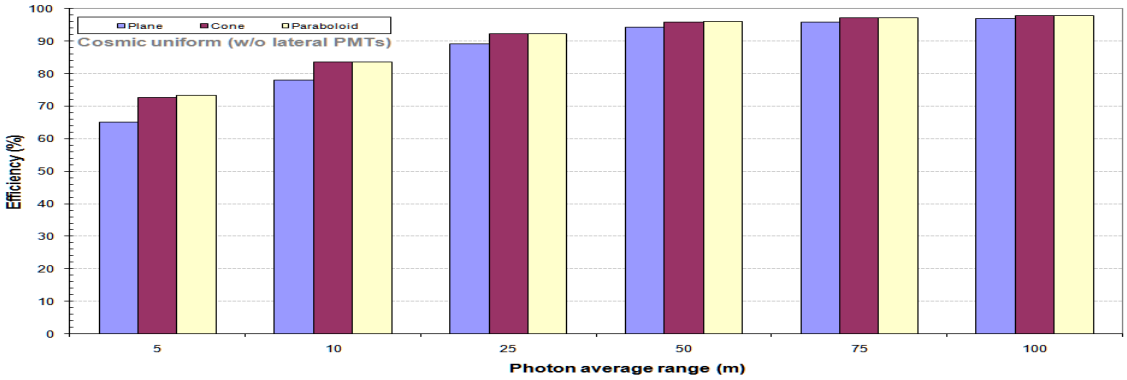

Figure 25: Efficiency for photons generated as cosmic rays with uniform distribution.

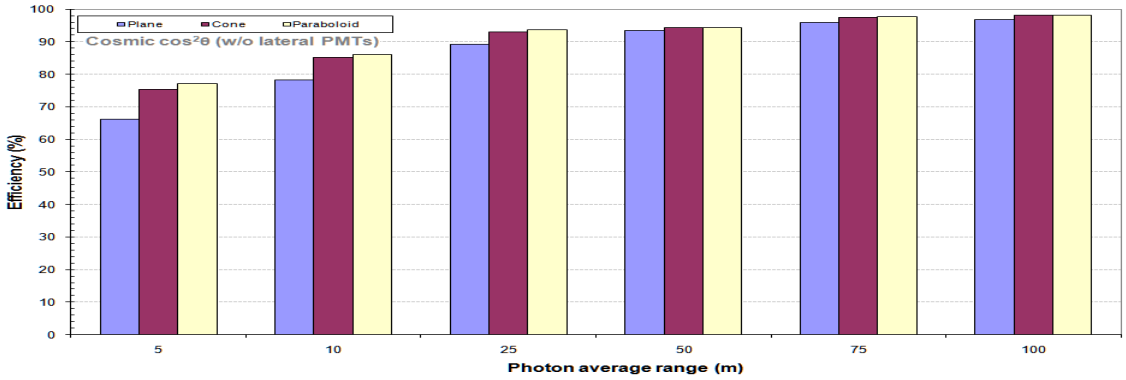

Figure 26: Efficiency for photons generated as cosmic rays with cos^2 distribution.

As a summary, Figures 27, 28 and 29 compare the detection efficiency for all the studied cases above. It becomes clear that, for the efficiency, lateral PMTs and internal structures around the PMTs are not essential for a photon average range higher than 25 m.

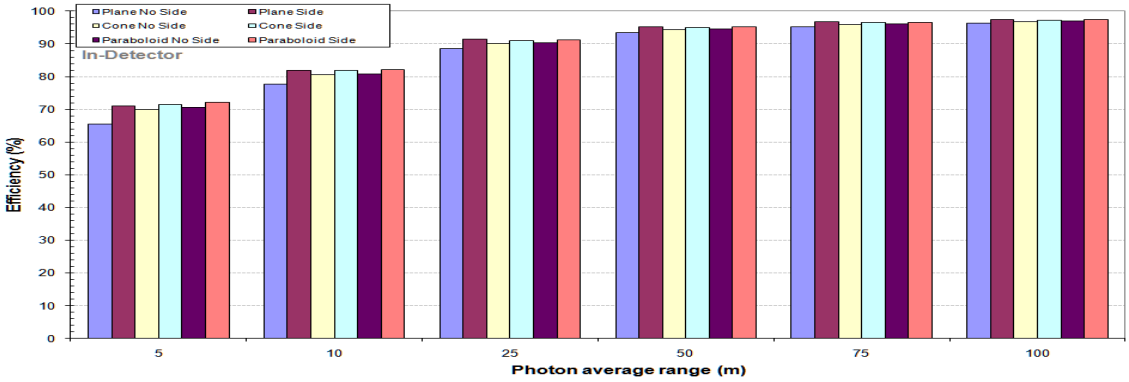

Figure 27: Efficiency for photons generated isotropically inside the detector.

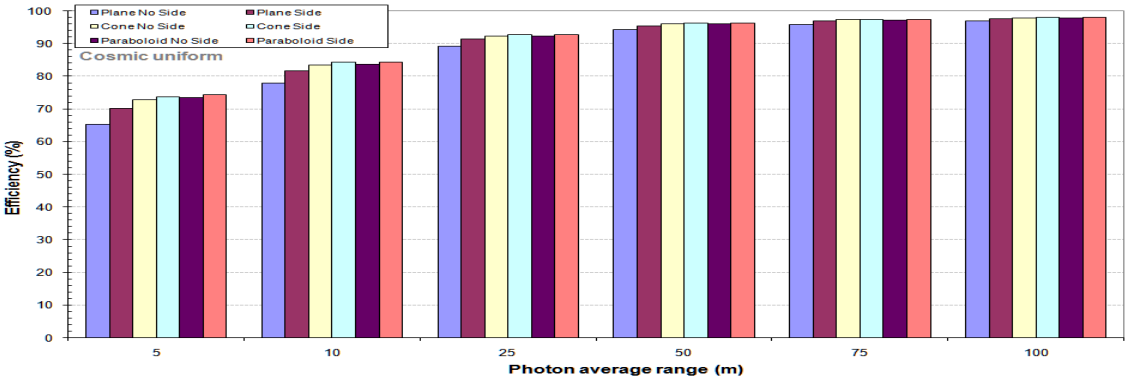

Figure 28: Efficiency for photons generated as cosmic rays with uniform distribution.

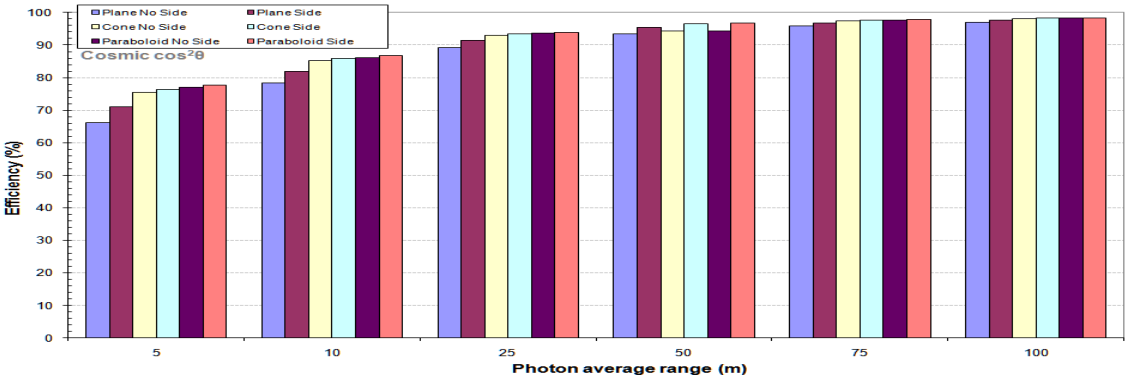

Figure 29: Efficiency for photons generated as cosmic rays with cos^2 distribution.

5 Conclusions

A ROOT based Monte Carlo simulation for light propagation inside the target volume detector of the Neutrinos-Angra project has been implemented. Based on this simulation, the following conclusions can be made: there is no practical difference between shifted and face-to-face top-bottom PMTs positioning; from the point of view of detection efficiency, internal structures (cone or paraboloid) and lateral PMTs are not essential for photon average range values higher than 25 m; the use of internal structures increases the bottom/top ratio, which may help on the cosmic rays veto system.

6 Acknowledgments

The Angra Neutrino Project relies mainly on financial support by FINEP, and also has important contributions from CNPq, FAPEMIG, FAPERJ, FAPESP, CAPES, and the PCI program of the Ministry of Science and Technology.

References

[1] J. Anjos et al. Brazilian Journal of Physics. Vol. 36, nro. 4A, 2006.

[2] *http://www.sales.hamamatsu.com/en/products/electron-tube-division/detectors/photomultiplier-tubes/part-r5912.php*

[3] A. F. Barbosa, *Simulation results for light propagation in the central detector: 2-dimensional case*, AngraNote **017-2011**, 2011.

[4] ROOT - A Data Analysis Framework, *http://root.cern.ch*

7 Appendix: Results Summary

With lateral PMT		In-Detector			
Internal structure	Average range (m)	Total efficiency (%)	Top (%)	Bottom (%)	Side (%)
Plane	5	70.92	42.02	41.84	16.14
	10	81.95	41.85	41.73	16.42
	25	91.36	41.65	41.62	16.73
	50	95.26	41.64	41.58	16.78
	75	96.73	41.62	41.52	16.86
	100	97.51	41.60	41.52	16.88
Cone	5	71.49	47.82	48.09	4.09
	10	81.82	47.74	48.00	4.26
	25	91.04	47.71	47.80	4.49
	50	95.03	47.70	47.65	4.65
	75	96.52	47.69	47.59	4.72
	100	97.31	47.68	47.57	4.75
Paraboloid	5	72.08	47.97	48.04	3.99
	10	82.15	47.87	47.92	4.21
	25	91.17	47.81	47.71	4.48
	50	95.14	47.74	47.63	4.63
	75	96.60	47.72	47.56	4.72
	100	97.41	47.73	47.52	4.75

Figure 30: Results summary for photons generated isotropically inside the detector.

With lateral PMT		Cosmic Uniform			
Internal structure	Average range (m)	Total efficiency (%)	Top (%)	Bottom (%)	Side (%)
Plane	5	70.16	28.79	53.47	17.74
	10	81.60	30.44	52.08	17.48
	25	91.42	31.67	50.86	17.47
	50	95.43	31.99	50.54	17.47
	75	96.84	32.12	50.39	17.49
	100	97.56	32.18	50.32	17.50
Cone	5	73.79	22.90	73.18	3.92
	10	84.25	25.47	70.69	3.84
	25	92.68	27.18	68.98	3.84
	50	96.17	27.71	68.41	3.88
	75	97.41	27.92	68.20	3.88
	100	98.00	28.03	68.07	3.90
Paraboloid	5	74.35	23.20	73.02	3.78
	10	84.31	25.38	70.82	3.80
	25	92.77	27.11	69.07	3.82
	50	96.24	27.63	68.51	3.86
	75	97.32	27.82	68.33	3.85
	100	97.95	27.92	68.24	3.84

Figure 31: Results summary for photons generated as cosmic rays with uniform distribution.

With lateral PMT		Cosmic cos			
Internal structure	Average range (m)	Total efficiency (%)	Top (%)	Bottom (%)	Side (%)
Plane	5	70.94	29.04	54.32	16.64
	10	81.96	30.88	52.55	16.57
	25	91.47	31.99	51.42	16.59
	50	95.39	32.36	51.06	16.58
	75	96.83	32.46	50.96	16.58
	100	97.60	32.96	50.59	16.45
Cone	5	76.25	18.80	78.15	3.05
	10	85.84	21.25	75.64	3.11
	25	93.46	22.94	73.89	3.17
	50	96.52	23.52	73.30	3.18
	75	97.60	23.70	73.09	3.21
	100	98.23	23.83	73.05	3.12
Paraboloid	5	77.78	19.56	77.46	2.98
	10	86.71	21.67	75.34	2.99
	25	93.90	23.33	73.68	2.99
	50	96.85	24.00	72.97	3.03
	75	97.82	24.22	72.73	3.05
	100	98.37	24.52	72.57	2.91

Figure 32: Results summary for photons generated as cosmic rays with $cos^2\theta$ distribution.

Without lateral PMT		In-Detector			
Internal structure	Average range (m)	Total efficiency (%)	Top (%)	Bottom (%)	Side (%)
Plane	5	65.52	49.86	50.14	0
	10	77.67	50.05	49.95	0
	25	88.59	50.05	49.95	0
	50	93.44	50.08	49.92	0
	75	95.30	50.10	49.90	0
	100	96.35	50.09	49.91	0
Cone	5	69.95	49.86	50.14	0
	10	80.50	49.87	50.13	0
	25	90.09	49.96	50.04	0
	50	94.34	50.04	49.96	0
	75	95.93	49.86	50.14	0
	100	96.82	50.07	49.93	0
Paraboloid	5	70.55	50.00	50.00	0
	10	80.81	50.05	49.95	0
	25	90.24	50.12	49.88	0
	50	94.46	50.13	49.87	0
	75	96.02	50.16	49.84	0
	100	96.91	50.19	49.81	0

Figure 33: Results summary for photons generated isotropically inside the detector.

Without lateral PMT		Cosmic Uniform			
Internal structure	**Average range (m)**	**Total efficiency (%)**	**Top (%)**	**Bottom (%)**	**Side (%)**
Plane	5	65.19	36.04	63.96	0
	10	77.95	38.10	61.90	0
	25	89.22	39.79	60.21	0
	50	94.17	29.26	70.74	0
	75	95.92	40.42	59.58	0
	100	96.86	40.52	59.48	0
Cone	5	72.74	24.13	75.87	0
	10	83.52	26.85	73.15	0
	25	92.31	28.69	71.31	0
	50	95.93	29.27	70.73	0
	75	97.26	29.50	70.50	0
	100	97.87	29.63	70.37	0
Paraboloid	5	73.39	24.44	75.56	0
	10	83.56	26.78	73.22	0
	25	92.36	28.65	71.35	0
	50	96.00	29.26	70.74	0
	75	97.17	29.47	70.53	0
	100	97.85	29.58	70.42	0

Figure 34: Results summary for photons generated as cosmic rays with uniform distribution.

Without lateral PMT		Cosmic cos			
Internal structure	**Average range (m)**	**Total efficiency (%)**	**Top (%)**	**Bottom (%)**	**Side (%)**
Plane	5	66.12	36.10	63.90	0
	10	78.34	34.83	65.17	0
	25	89.30	39.79	60.21	0
	50	93.45	40.32	59.68	0
	75	95.94	40.45	59.55	0
	100	96.89	40.58	59.42	0
Cone	5	75.41	19.71	80.29	0
	10	85.20	22.37	77.63	0
	25	93.10	24.24	75.76	0
	50	94.37	24.89	75.11	0
	75	97.42	25.10	74.90	0
	100	98.04	25.25	74.75	0
Paraboloid	5	77.04	20.40	79.60	0
	10	86.16	22.66	77.34	0
	25	93.60	24.44	75.56	0
	50	94.41	25.17	74.83	0
	75	97.67	25.41	74.59	0
	100	98.24	25.54	74.46	0

Figure 35: Results summary for photons generated as cosmic rays with $cos^2\theta$ distribution.